Mohamed Khider University of Biskra
Faculty of exact sciences
Matter Sciences department

MASTER MEMORY

Materials Science
Chemistry
Materials Chemistry

Réf. :

Presented by:
Meddas zakaria

02-06-2025

Physical and chemical properties of spinal oxide doped with magnesuim

---

Jury:

Dr	Chadli Ilhem	MCB	Université de Biskra	President
Dr	Omari Elies	MCA	Université de Biskra	Examinateur
Dr	Tebermacine ouarda	MCB	Université de Biskra	Rapporteur

AcademicYear:2025/2024

Acknowledgements

I praise and thank Allah Almighty for His guidance and support throughout my academic journey, and for granting me the strength and patience to complete this work.

I express my deepest gratitude and sincere appreciation to my supervisor, Dr. Tebermacine ouarda for her continuous guidance, scientific support, and valuable advice that greatly contributed to the success of this research.

I would also like to extend my heartfelt thanks to the members of the thesis committee, Dr. Chadli Ilhem and Dr. Omari Elies for accepting to review and evaluate this work, and for devoting their precious time to its assessment.

My sincere thanks go to all the professors who taught and supported me during my years of study, as well as to all the staff of the laboratories of the Department of Materials Science – Mohamed Khider University of Biskra**,** for their kind cooperation.

I would also like to give special thanks to all my fellow students and colleagues whose sincere support and encouragement were invaluable throughout this journey.

Dedication

To those who planted strength in my heart and perseverance in my soul...

To my beloved mother, the source of endless care, and to my dear father, my greatest support in life I dedicate this work as a token of gratitude and appreciation for everything you have done for me.

To my dear brothers and sisters, who have always been by my side, encouraging and supporting me may God bless you always.

To my loyal friends, who accompanied me throughout this journey of learning —
thank you for every sincere moment and every shared smile.

And to everyone who left a positive mark on my life, this work is humbly dedicated to you, with love and gratitude.

List of Figures

CHAPTER I

CHAPTER II

CHAPTER III

List of tables

Table of Contents

General Introduction

General Introduction

Spinel ferrites, with the general formula **AB_2O_4**, are a class of crystalline materials known for their remarkable chemical and thermal stability. These compounds have attracted extensive attention due to their wide range of applications in various technological and industrial fields. Spinel ferrites are commonly utilized in magnetic recording media**,** magnetic fluids**,** MRI enhancement**,** magnetically guided drug delivery**,** sensors, and pigments, among others.[1]

One of the notable members of the spinel family is calcium ferrite ($CaFe_2O_4$)**.** It is considered particularly important due to its natural abundance, eco-friendly nature, and non-toxic behavior. Calcium ferrite nanoparticles (CFNPs) exhibit superparamagnetic properties and are known to function as efficient catalysts. Furthermore, CFNPs have been extensively studied for their adsorption performance in removing dyes from aqueous solutions, offering a more environmentally safe alternative compared to other ferrite materials.[2]

In this work, we aim to study the chemical and physical properties of calcium ferrite, covering several branches of chemistry. The compound $CaFe_2O_4$ will be synthesized using the sol-gel method, and characterized by techniques such as X-ray diffraction (XRD)**,** Fourier-transform infrared spectroscopy (FTIR)**,** and ultraviolet-visible (UV-Vis) spectroscopy. This study will focus on understanding the structural, optical, and functional properties of the synthesized material.

Reference

[1] S. K. Pardeshi, R. Y. Pawar, Optimization of reaction conditions in selective oxidation of styrene over fine crystallite spinel-type $CaFe_2O_4$ complex oxide catalyst, Materials Research Bulletin 45(5), 609–615 (2010)

[2] N. Yadav, M. Ahmaruzzaman, Recent advancements in $CaFe_2O_4$-based composite: Properties, synthesis, and multiple applications, Energy & Environment 35(1), 458–490 (2024)

Chapter I: Bibliographic Study

I.1. Introduction

Spinel ferrite materials are metal oxides exhibiting a spinel crystal structure, typically represented by the general formula AB_2O_4, where A and B are different metal cations occupying tetrahedral (A site) and octahedral (B site) positions, respectively. The nature, quantity, and spatial distribution of these cations within the crystal lattice greatly affect the physicochemical properties of ferrites.

Nanocrystalline magnetic materials have gained significant attention across various scientific fields—including physics, chemistry, biology, medicine, materials science, and engineering—due to their unique and remarkable properties. Nanomaterials are defined by particle sizes up to 100 nanometers and exhibit a high surface-to-volume ratio, which enhances or alters their reactivity, as well as their thermal, mechanical, optical, electrical, and magnetic behaviors compared to their bulk counterparts. While the properties of bulk morphology, and composition of nanomaterials collectively determine their overall characteristics.

Moreover, these properties can be finely tuned by modifying the particle size and chemical makeup. Spinel ferrites are considered highly valuable and intriguing from both practical and theoretical standpoints. Nanoparticles of ferrites such as $CoFe_2O_4$, $MnFe_2O_4$, $CuFe_2O_4$, $ZnFe_2O_4$, and $NiFe_2O_4$ have attracted widespread interest due to their thermal and chemical stability, as well as their diverse structural, magnetic, optical, electrical, and dielectric characteristics. These properties make them suitable for a wide range of applications, including photocatalysis, photoluminescence, biosensing, humidity sensing, catalysis, magnetic refrigeration, permanent magnets, drug delivery, and magnetic hyperthermia.[1]

The different types of spinel compounds—normal, inverse, and mixed spinels—will be covered in detail in this chapter along with their crystal structures. Since cation

vacancies and ionic substitutions are important factors in determining the physical and chemical properties of these materials, special attention will be paid to any crystallographic defects that may arise within their structure.

This chapter will also examine the different applications of spinel compounds in a variety of technological domains.

I.2 General Description

I.2.1. The Spinel Structure

Bragg and Nishikawa made the initial determination of the structure of Spinal as they existed for MgAl2O4 in 1915. Among inorganic materials, the spinel structure is regarded as one of the most varied and stable crystal structures. It has the general formula AB_2X_4, in which X stands for anions like oxygen, sulphur, or selenium, and A and B for metallic cations. Because of its remarkable physical characteristics and capacity to hold different cations at different lattice sites, the mineral $MgAlO_4$ is considered the canonical example of the spinel structure, and its crystal structure has been thoroughly investigated. The majority of spinel compounds are members of the $Fd\bar{3}m$ space group (No. 227) and crystallise in a face-centered cubic (FCC) form. Eight formula units—32 anions and 24 cations—make up a single unit cell, which has 56 atoms overall.
The foundation of these crystal systems is a nearly perfect cubic close-packed (ccp) anion sublattice. There are 96 interstitial spaces between the anions in the unit cell, but only 24 of them are filled by cations:
The tetrahedral coordination sites are occupied by 8 cations (8a).
Half of the octahedral coordination sites (16d) are occupied by 16 cations.[2]

We denote **a** as the lattice parameter of the cubic unit cell. To describe its structure, the unit cell (with parameter a) is divided into eight smaller cubes, called octants, each with an edge length of **a/2**. Figure I.1 illustrates the positions of the cations and anions . The oxygen anions are arranged identically in all octants: they occupy the vertices of a tetrahedron that fits within a cube of edge length **a/4**. The occupied A sites are found at the centers of alternating octants and on half of the vertices of all octants. These A sites form

two face-centered cubic (f.c.c.) sublattices that are offset from each other by **a/4** along the [111] crystallographic direction.

The B sites that are occupied are located in every second octant. Like the oxygen atoms, they are positioned at one-quarter the length of the octant's diagonal, starting from four of its eight corners. These B sites also form a tetrahedron inscribed within a cube of edge length **a/4**.[3]

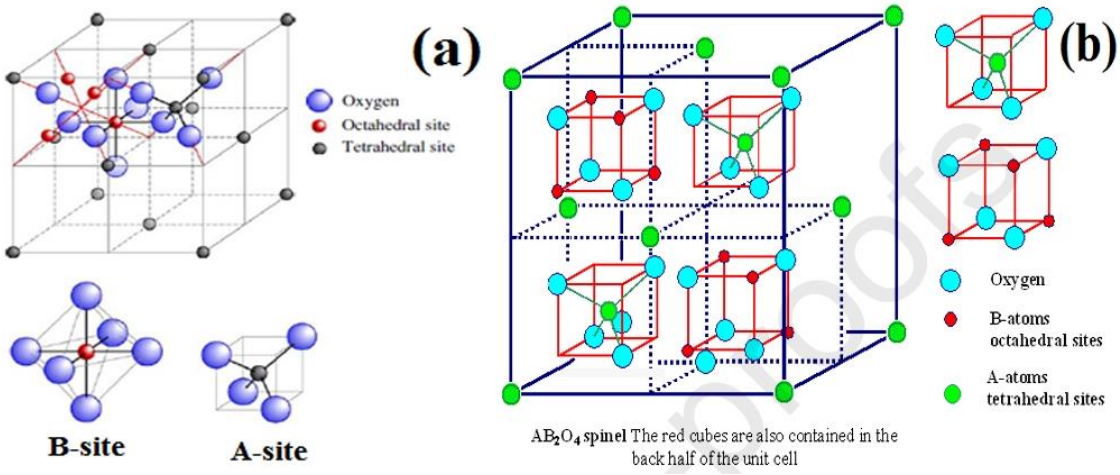

Fig.I.1: Typical Spinel Crystal structure Showing Tetrahedral and Octahedral Cation Sites.[4]

I.2.2 Space Groups and Point Symmetry

The spinelle mineral is (Mg2+)A[Al2+3]BO4. It serves as a reference to the structure description. The content of sites A and B is indicated by parenthesis and crochets, respectively. The space group of MgAl2O4 is group number 227, Fd3¯m. This group has

two origins and is described in international tables. According to disposition 1, the origin is 3¯m, or on site B. The oxygen atom coordinates in this description are (u, u, u) (3/8 3/8 3/8). The origin is located at 4 Å 3 m on site A in disposition 2. This disposition is derived from the first by translating (-1/8 -1/8 -1/8). [5]

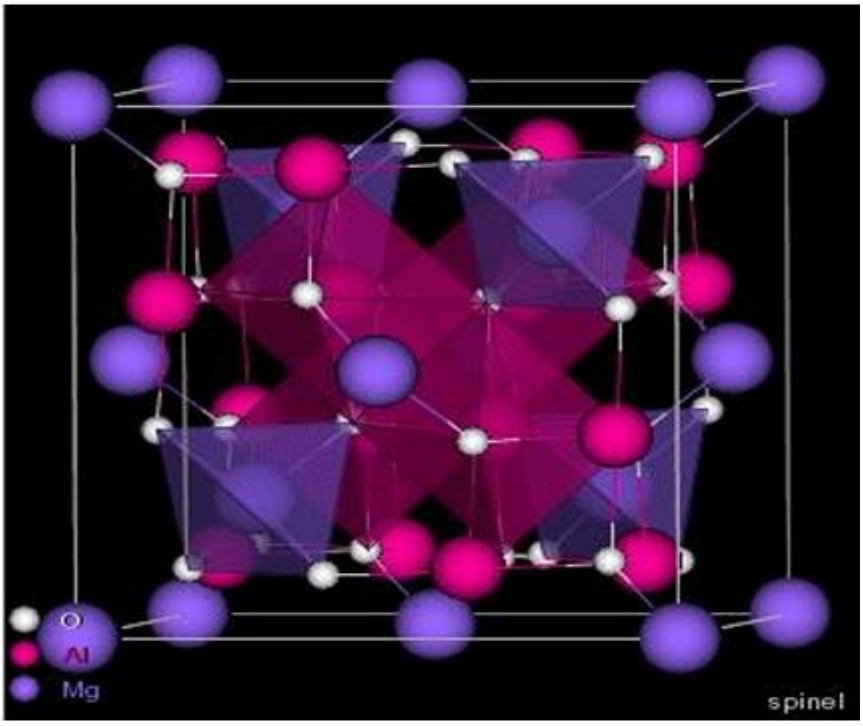

Fig. 1.2: Crystallographic Structure of $MgAl_2O_4$ Spinel [3]

I.2.3. The Spinel Superstructure: Long-Range Cation Ordering

The arrangement of cations within a sublattice occurs randomly; however, when a sublattice contains multiple types of cations, the formation of long-range cation order or superstructure has been observed. A compilation of various spinel superstructures is presented in Table 1.4. At least five unique types have been recognized, displaying 1:1 or 1:3 ordering at the A sites, as well as 1:1 or 1:3 ordering at the B sites. This long-range cation order shows certain similarities to the order-disorder phenomena observed in alloys [6].

Tableau I.1 : Spinel Superstructure [6]

Composés	Sites tétraédriques	Sites octaédriques	
$Zn(LiNb)O_4$	Zn	Nb Li	O_4
$V^V(LiCu)O_4$	V	Li Cu	O_4
Fe_3O_4	Fe^{3+}	Fe^{2+} Fe^{3+}	O_4
$Zn_2Ge_3O_8$	2 Zn	3Ge □	O_8
$LiZn(LiGe_3)O_8$	Li, Zn	3Ge Li	O_8
$Co_3(Vo_4)_2(Iow)$	2V	3Co □	O_8
$LiGaTiO_4$	2Ga, Li	3Ti, Ga, 2Li	O_{12}

□ : Lacune

I.3. The Different Types of Spinels

Three different types of spinelle-structured compounds can be distinguished by the way that cations are distributed on tetraédrique and octaédrique sites.

I.3.1. Normal Spinel

The type of site occupied by this spinelle is (Td)[Oc], and its formula is (A)[B]2O4.2O4(Td: tétraédrique, Oc: octaédrique): two atomes B are in octaédrique sites, while one atome A is in a tétraédrique site. Is this a direct or normal distribution?

I.3.2. Inverse Spinel

This spinelle's formula is (B) [AB]. O4 and the site type occupied is (Td) [Oc] 2 O4: an atome of A and an atome of B are in octaédrique sites, whereas an atom B is in a tétraédrique site. This is an inverse or reversible spinelle, with half of the ions trivalents occupying the tétraèdres and the other half of the same trivalent and divalent ions occupying the octaèdres. [7]

I.3.3. Mixed Spinel

The distribution of cations over the two sites is more complicated in many cases. Then, we talk about mixed spinelles.

I.3.4 the inversion rate:

Tetrahedral and octahedral interstitial sites are made possible by the presence of $O2^{-}$ ions within the face-centered cubic (FCC) lattice. This allows for a variety of cation distributions among these crystallographic sites.
The inversion degree (λ) is a parameter that can be used to describe these cationic configurations.Such a spinel oxide's general chemical formula is as follows: $(A_{1-2}\lambda^{2+}B_{2}\lambda^{3+})[A_{2}\lambda^{2+}B_{2-2}\lambda^{3+}]O_{4}^{2-}$ Where The degree of cation redistribution between tetrahedral and octahedral sites is indicated by the inversion degree, denoted by λ. With varying structural implications, the value of λ falls between 0 and 0.5. When λ = 0, the spinel is known as normal, and its chemical formula is $A^{2+}B_{2}^{3+}O_{4}$. When 0 < λ < 0.5, the spinel is regarded as partially inverted. λ = 0.5: The chemical formula for spinel, also known as inverse, is $B^{3+}(B_{0.5}^{3+}A_{0.5}^{2+})_{2}O_{4}$.[8]

I.4. Defects in the spinel structure

Defects in spinel materials can be caused due to low cations at site A, in the presence of site B, as well as from low or high oxygen levels. Before diving into specifics on this topic, a general summary of the ponctuels' defects during the crisis is necessary.

I.4.1. Point defects

In the simple case of an ordered crystal, several types of defects can be described, as illustrated in Fig. I.2.":

A lacuna : is defined as the absence of an atom, sometimes referred to as a vacancy. A cationic gap in a crystal produces a negative charge.

Interstitial: The presence of a network of atoms among the atoms. Solution solide interstitielle refers to the existence of a foreign atom within the lattice of atoms.

Substitution: A solid substitution transpires when an exterior atom replaces a network atom.

Electrical charge failure: One crystal site has a negative charge (free electron) or a larger positive charge (trou d'électron) than other sites of the same kind.

Anti-site defects: If the crystal is ordered, meaning it is formed of several atom types with a tight chemical alternation, it may have anti-site defects, which are atomes that are located well in an area of the réseau but that break chemical regularity.

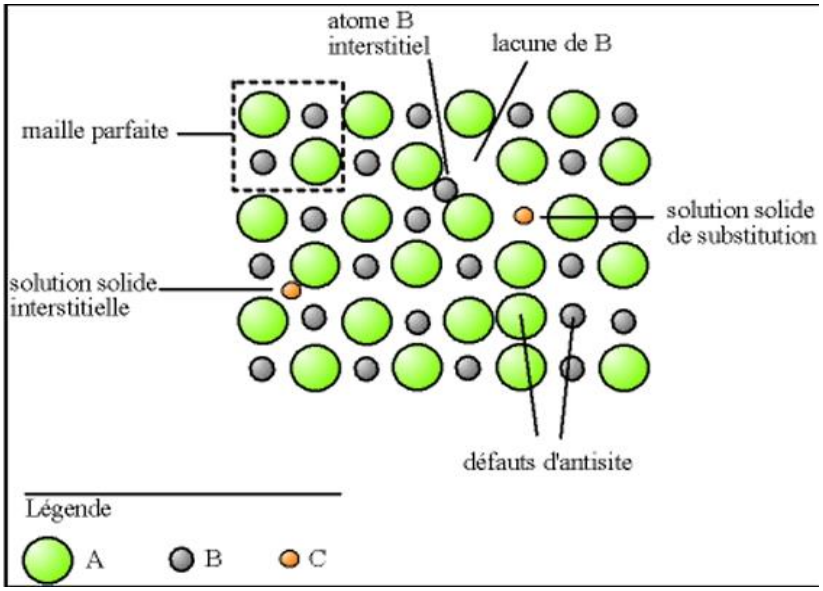

Fig. I.3: Types of Point Defects in an Ordered AB-Type Crystal [3]

I.4.2. association of point defects

Schottky defect : represents the combination of an anionic and a cationic lacune in ionic crystals.

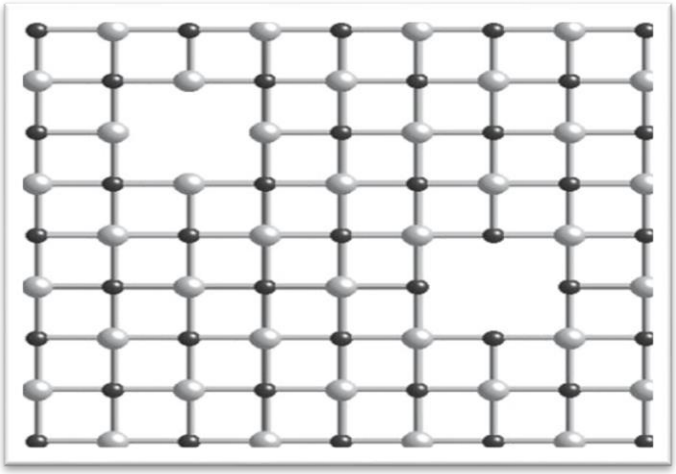

Fig. I.4: Image of a Schottky Defect (Vacancy)[9]

Frenkel defect : An atome leaves its usual location and enters an interstitial position. Because cations are smaller than anions, they are the only ones that can produce an ionic crystal.[3]

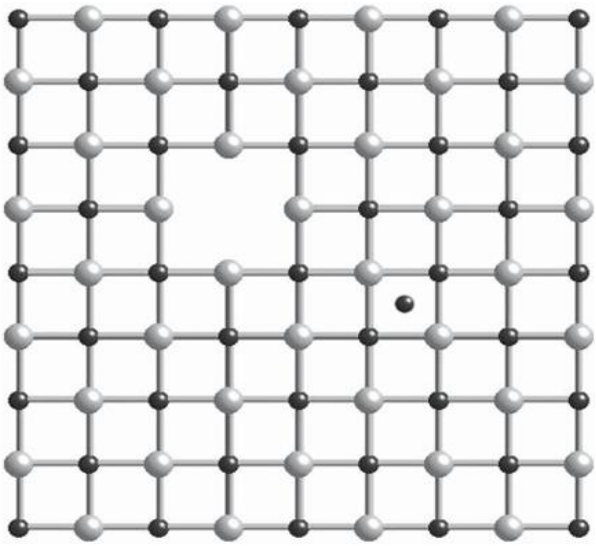

Fig. I.5: Image of a Frenkel Defect[9]

I.5.Spinel Properties

I.5.1. Optical Properties

Spinels are characterized as transparent substances across both the visible and mid-infrared spectrum (0.2 - 6 pm) 13. In addition to exhibiting optical isotropy, they possess a refractive index ranging from 1.712 to 1.736; conversely, Gahnites display a greater refractive index approaching 1.780 [10,11]. Spinels exhibit allochromatism, meaning they acquire coloration from metal ions (transition elements) present in minimal amounts, which results in color variation contingent upon their concentration within the material [12-14].

Cr3+ (in octahedral coordination) yields red and pink hues.

Fe3+ (in octahedral coordination) manifests as green.

Fe2+ (in tetrahedral coordination) produces blue and purple shades.

I.5.2. Electronic properties

The phenomenon of electronic conduction within spinel frameworks is enhanced through the process of electron transitions that transpire between cations located in equivalent crystallographic positions [15]. Consequently, when evaluating the spatial separation among these sites, electronic transfers primarily occur between cations situated within the octahedral sites. Indeed, the interstitial distance that separates two octahedral sites is inferior to that which distinguishes two tetrahedral sites or two sites exhibiting differing characteristics. [13 ,16,17]

I.5.3. Magnetic properties

The magnetic characteristics inherent to spinel structures have engendered considerable debate within the scholarly literature. Numerous investigations have demonstrated that inorganic materials exhibiting the AB2X4 spinel architecture have captivated the interest of physicists for an extended duration, as the configuration of their B-site lattice (tetrahedral site) impedes the inherent tendencies of charge distribution and spin alignment [18].

I.5.4. Optoelectronic properties

The optoelectronic characteristics of spinel-like oxides (OMTs), akin to the majority of transition metal oxides, exhibit a direct correlation with their band structure configurations. Typically, the valence band (BV) is composed of fully occupied oxygen orbitals (2p6 orbitals), whereas the conduction band (BC) predominantly consists of unoccupied 3d cation orbitals, as evidenced by the band gap value illustrated in Figure I.7

[10].

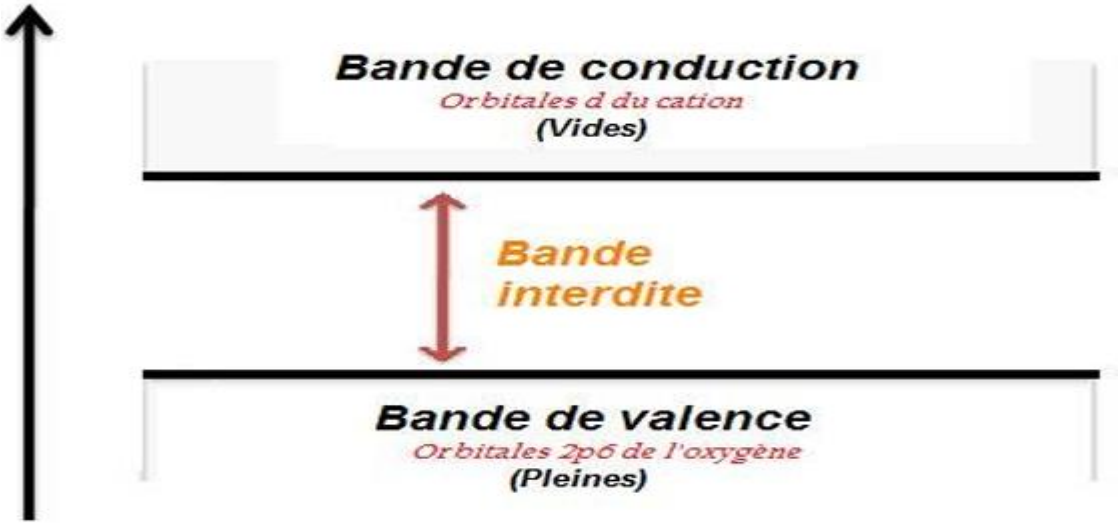

Figure I.7: Simplified representation of the band diagram [19]

I.6. Applications of the spinel structure AB_2O_4

Intrudction

Metal ferrites like nickel ferrite, copper ferrite, zinc ferrite, cobalt ferrite, and other ferrites are highly abundant and used as catalysts in various transformations. However, CaFe2O4 is the most abundant alkali metal ferrite, which is eco-friendly and non-toxic. CaFe2O4 is a superpara magnetic material that can be easily recovered from the reaction media due to its magnetic properties. Therefore, it has been widely used in numerous applications, such as dye degradation, removal of heavy metal ions, transesterification reaction, gas sensing, photocatalytic water split ting, drug delivery, etc.[20]

These applications may fall under a number of different categories:

Catalyse: One of the most advantageous families of crystallin compounds that can be employed as catalysts is the AB2O4 family. Many methods have been used to logically adjust the spinelles' physical and chemical characteristics, including their composition,

structure, morphology, flaws, and substrates. This adjustment may result in spinelles with enhanced catalytic activity, which may further speed up explosive piles, metal-air batteries, and water separation devices, extending their lifespan and lowering polarization.[21]

Gas sensing : Poisonous gas sensing has always been a top issue in pollution management, industry, the defense sector, and medical diagnosis. Gas sensing is also necessary for the daily life of human beings, not only beneficial to these industries.121 Researchers are looking for sensing devices with exceptional selectivity, excellent sensitivity, recovery speed, rapid response, and porous structure.122 Therefore, CFNCs were employed as cost-effective gas sensors with excellent efficiency, for poisonous gases like HCHO, isoprene, etc

Formaldehyde (HCHO) is a toxic gas that is dangerous to human health. Researchers have looked at the gas-sensing capabilities of the CF to HCHO conversion. The CF-based sensor has an increased gas response (16.50), a rapid response-recovery time (153, and 54 s), excellent mois ture resistance, and long-term stability, among other characteristics. This one-of-a-kind CF nano cube has the potential to be exploited as a promising HCHO gas detection material. When inhaled in high concentrations, formaldehyde may cause cancer and congenital disabilities in humans. Even at low concentrations, HCHO shows teratogenic and carcinogenic behavior and may cause significant health issues in humans. Indoor ornamental elements progressively emit for maldehyde, which accumulates in the space. As a result, creating sensitive formaldehyde sensors is critical for preserving the indoor environment and human health.[20]

Références

[1] Salih S. J., Mahmood W. M., Review on magnetic spinel ferrite (MFe_2O_4) nanoparticles: From synthesis to application, Heliyon, Volume 9, Issue 6, Article e16601 (2023).

[2] Sickafus K. E., Wills J. M., Grimes N. W., Structure of Spinel, Journal of the American Ceramic Society, Volume 82, Issue 12, Pages 3279–3292 (1999).

[3] Tibermacine W., Structural study and properties of spinel-type oxides $Ni_{1-x}Fe_xAl_2O_4$, Doctoral dissertation, Mohamed Khider University of Biskra, Algeria (2019).

[4] Narang S. B., Pubby K., Nickel Spinel Ferrites: A review, Journal of Magnetism and Magnetic Materials, Volume 519, Article 167163 (2021).

[5] Meslem M., Electronic structure and magnetism in the spinel material $NiFe_2O_4$, Master's thesis, Mohamed Boudiaf University, M'sila, Algeria (2019).

[6] Long G. J., Grandjean F., Mössbauer spectroscopy and its applications to inorganic chemistry, in: Mössbauer Spectroscopy Applied to Inorganic Chemistry, Volume 3, Chapter 3, Plenum Press, New York (1989).

[7] Krupicka S., Novak P., Ferromagnetic Materials, Volume 3, North-Holland, Amsterdam (1982).

[8] Valenzuela R., Magnetic Ceramics, Instituto de Investigaciones en Materiales, Universidad Nacional Autónoma de México

[9] Coleman V. A., Jagadish C., Chennupati J., Stephen P., Thin Films and Nanostructures, Oxford: Elsevier Science Ltd., Pages 1–20 (2006).

[10] Kim S.-K., Jeong S.-Y., Cho C.-R., Magnetic properties of ZnO-based diluted magnetic semiconductors, Applied Physics Letters, Volume 82, Issue 4, Pages 562–564 (2003).

[11] Kogure T., Bando Y., Microstructure analysis of magnetic ceramics, Journal of Electron Microscopy, Volume 47, Issue 2, Pages 135–141 (1998).

[12] Carter C. B., Norton M. G. (Eds.), Point Defects, Charge, and Diffusion, in: Ceramic Materials: Science and Engineering, Springer, Pages 181–200 (2007).

[13] Benaouad A., Study of the electronic and optical properties of spinel group material (Galaxite), Master's thesis, University of Mostaganem, Algeria (2018).

[14] Liao Y. C., Du C. H., Xu F., Wang M. J., Wu C., Hsu Y. Y., Wu M. K., Superconductivity and structure in high-temperature phases, Physica C: Superconductivity, Volumes 369–371, Pages 886–890 (2004).

[15] Lebid M., Study of the influence of synthesis conditions on the physicochemical properties of the $LaFeO_3$ system, Doctoral dissertation, University of Biskra, Algeria (2012).

[16] Schiferl D., Waskowska A., High-pressure phase transition of perovskite-type oxides, Physical Review B, Volume 68, Article 094101 (2003).

[17] Hoshia T., Aruga Katoria H., Kosaka M., Takagi H., Magnetization and structure of spinel ferrites, Journal of Magnetism and Magnetic Materials, Volume 310, Pages e448–e450 (2007).

[18] Jouenne C. A., Traité de céramique et matériaux minéraux, Éditions Septima, Paris (1990).

[19] Yunus S. M., Shim H.-S., Lee C.-H., Asgar M. A., Ahmed F. U., Zakaria A. K. M., Magnetic behavior of substituted ferrites, Journal of Magnetism and Magnetic Materials, Pages 40–50 (2002).

[20] Guemache A., Synthesis and electrochemical properties of the $La_{1-x}M_xAlO_3$ system (M: Sr, Ca), Doctoral dissertation, University of Biskra, Algeria (2017).

[21] Hill R. J., Craig J. R., Gibbs G. V., Systematics of the spinel structure type, Physics and Chemistry of Minerals, Volume 4, Issue 4, Pages 317–339 (1979).

[22] Amiri L., Boceiri M., Boulakhras A., Structural study and spectroscopic characterization of mixed spinel-type oxides, Master’s thesis, University of Tiaret, Algeria (2020).

[23] Yadav N., Ahmaruzzaman M., Recent advancements in $CaFe_2O_4$-based composite: Properties, synthesis, and multiple applications, Energy & Environment, Volume 35, Issue 1, Pages 458–490 (2024).

[24] Krimmel A., Tsurkan V., Sheptyakov D., Loidl A., Magnetic and structural properties of complex oxides,

Chapter II: Experimental Techniques for Synthesis and Characterization

II.1. Methods for preparing spinel oxides

II.1.1Introduction

This chapter first presents the various experimental techniques for the preparation of mixed oxides :

→ Sol-gel method.
→ Co-precipitation method.
→ Solid-state synthesis method.

The second part presents the various techniques used to characterize spinel oxides:

→ X-ray diffraction (XRD).
→ Infrared spectroscopy

II.1.2 Sol-gel method

II.1.2.1 Synthesis by the Sol-gel method

The sol-gel process involves the synthesis of inorganic polymers or ceramics from a solution, transitioning from liquid precursors to a colloidal solution (sol) and ultimately forming a network structure known as a gel. This is a widely recognized and highly favored technique for synthesizing nano-ferrites and related composites. The sol-gel technique is efficient and cost-effective, producing extremely pure and crystalline nanomaterials with a uniform size distribution . It is commonly referred to as sol-gel auto-combustion, sol-gel autoignition, sol-gel self-combustion, low-temperature self-combustion, auto-ignition or self-propagation, and gel-thermal breakdown. In this process, stoichiometric amounts of metal precursors are dissolved in minimum amount of distilled water followed by the addition of an appropriate organic fuel (chelating/combustion agents), such as citric acid (C6H8O7), urea (CH4N2O), glycine (C2H5NO2), ethylene

glycol (C2H6O2), hydrazine (N2H4), carbohydrazide (CH6N4O), alanine (C3H7NO2), acetic acid (CH_3COOH) and acrylic acid (C3H4O2), hexamethylenetetramine (C6H12N4), polyvinyl alcohol (C2H4O)n, etc. The pH of the resulting solution is further modified by the addition of dilute ammonia solution (NH4OH). The solution is permitted to evaporate until gels are generated, which, upon continuous heating, undergo combustion to yield a solid powder. The solid powder is annealed in a furnace at various temperatures. Among these fuels, citric acid is the most widely employed for the manufacture of a large variety of spinel ferrites. It is cheap and is a more effective com plexing agent than hydrazine and glycine in making fine ferrite powder with smaller particle size . In general, a suitable fuel should react non-violently, produce harmless gasses and behave as a complexant for metal ions . The efficacy and manufacture of high quality fine powder depends on the kind of fuel, fuel to oxidizer ratio, precursors' concentration, pH, agitation, heating mechanism, annealing tempera ture and the preparation condition . [1]

II.1.2.2 Precursors:

The precursor operates as a chemical agent that promotes the commencement of the reaction. It generally presents itself as an alcoholate (an alkoxide symbolized by the formula M (OR) n, where M indicates a metal such as silicon or zirconium, while R denotes an organic alkyl moiety CnHn-1) or as a metallic salt. Two distinct methodologies for Sol-gel synthesis are recognized:

II.1.2.2.1Inorganic or colloidal route:

This technique is based on metal salts (which include chlorides, nitrates, and oxychlorides) that are solubilized in an aqueous environment. Despite the economic benefits associated with this pathway, it poses significant challenges regarding controllability, which limits its applicability. Nonetheless, it continues to be the favored technique for the synthesis of ceramic materials**.**

II.1.2.2.2. Metallo-organic or polymeric route:

This method is accomplished through the employment of metal alkoxides in organic solvents. Although this approach tends to incur higher costs, it provides enhanced control over particle dimensions. The aqueous route facilitates the generation of gels

composed of particles commonly referred to as hydrogels, whose structures are often thoroughly characterized and whose chemical composition aligns with a hydrated oxide: MoX, nH2O (this nomenclature encompasses oxo-hydroxides and hydroxides). The Sol-Gel reaction transpires through a two-step process: the initial formation of the “soil” followed by the subsequent development of the “gel” . [2]

II.1.2.3 Advantages and disadvantages of the sol-gel process

The benefits associated with the sol-gel process are as follows:

- Minimal energy expenditure: the vitrification or sintering of dry gels can be accomplished at temperatures lower than those typically employed in industrial applications using conventional raw materials.
- Streamlined execution: the inherent viscosity of sols and gels facilitates the direct production of materials in diverse forms, including thin films, fibers, fine powders, and bulk materials.
- Customizable materials: the regulation of condensation reactions permits the directed polymerization and enhancement of material properties tailored to specific intended applications.
- Elevated purity levels and enhanced uniformity of the resultant material.
- The capability to deposit thin films on both surfaces of a substrate within a singular operation.
- The achievement of multi-component coatings in a single procedural step.

The constraints associated with the sol-gel process are as follows:

- Elevated expenses associated with alkoxide precursors.
- Challenges in maintaining process control and the prolonged duration of the procedure, necessitating the manipulation of substantial volumes of solvents.

- A significant limitation is the minimal thickness of the resultant layers, necessitating multiple cycles of deposition and drying to achieve thicknesses on the order of several hundred nanometers, thereby increasing the likelihood of cracking due to the sequential drying of the initially deposited layers, which heightens the risk of electrical short.[3]

II.1.3. Synthesis by solid-state reaction (dry route synthesis)

The mechanism of spinel ferrite synthesis by solid-state reactions has been discussed by numerous researchers based on simple diffusion couple involving the iron and metal salts. In this procedure, the desired composition is usually created from the suitable amount of raw mineral oxides or carbonates by crushing, grinding and milling. The overall preparation process normally contains four basic processes; (1) Preparing a combination of required composition, (2) Pre sintering the mixture to generate ferrite, (3) Converting the raw ferrite into powder and pressing the powder, and (4) Sintering. This process suffers from un controlled stoichiometry, poor composition, chemical inhomogeneity, contamination, coarser particle size, and introduction of contaminants during grinding and high annealing temperature. In this situation, wet chemical techniques have emerged as savior and offer ferrite nanoparticles with reproducible stoichiometric composition and appropriate microstruc tures.[4]

II.1.4. Co-precipitation method

The synthesis of Spinal by coprecipitation method is the most convenient, economic, and less time-consuming, has high mass production, and is widely employed among all other methods in order to create uniform-sized particles . This approach is also commonly used to synthesis biocompatible SFs, which have uses in in vivo biomedical area . This approach involves the mixing of aqueous solutions of divalent and trivalent transition metal salts that are uniformly mixed together in 1:2 mole ratios with continuous and vigorous stirring in an alkaline medium. The coprecipitation approach demands careful monitoring of pH in order to obtain high-quality Spinal . The main downside of this

method is that relatively poor crystallinity of synthesized SFs and consequently a subsequent heat treatment is necessary in order to achieve greater crystallinity. This approach is preferred to be the suitable route for synthesizing water-dispersible SFs , and a variety of SFs have been synthesized by coprecipitation method including CoFe2O4 , MnFe2O4 , Fe3O4, and Sn-doped MnFe2O4.[5]

II.2. Characterization techniques of spinel oxides

II.2.1 X-ray diffraction

II.2.1.1 X-ray diffraction – Powder method

The X-ray diffraction technique is recognized as the most commonly used method in materials science for the analysis and structural characterization of materials, thus allowing for the assessment of their crystalline structure and the identification of existing phases. The material may be found in the form of powder, solid, or thin films. The X-ray tube utilized in the X'Pert Panalytical diffractometer is equipped with a copper anticathode. Detection is accomplished with a silicon lithium detector paired with a multi-channel analyzer, which enables the selection of the KCu line (=1.5402Å). Its fundamental principle revolves around capturing the rays that are diffracted by a sample as a function of the angle between the incoming radiation and the sample itself. The X-ray beam collected by the detector accurately reflects the combination of the individual peaks diffracted by each coherent diffraction domain. The determination of the interplanar distance of the crystal planes, indicated by the Miller index (hkl) of the crystal lattice, is made possible through X-ray diffractometry and the application of Bragg's law [6] . Figure II.7

$$2\, d_{(hkl)} \sin(\theta_{hkl}) = n\, \lambda$$

λ: Wavelength of the incident X-ray beam.

θ: Bragg angle.

$d_{(hkl)}$: Interplanar spacing (inter-reticular distance) of a family of crystal planes indexed by Miller indices (hkl).

n: Integer number (order of diffraction)

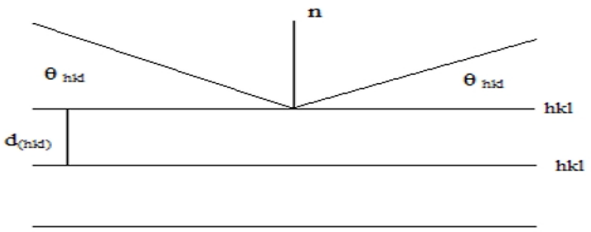

Figure II.7: Diagram of Bragg's Law

Alongside identifying the crystallochemical characteristics and the crystal structure of the phases present in the powder, the Scherrer model—utilizing peak broadening—establishes a direct correlation between the diffraction peaks and the average crystallite size [7]

$$d=B\lambda/\beta\cos\theta_{hkl}$$

d: The average crystallite size.

β: The full width at half maximum (FWHM) of the peak.

$\theta_{(hkl)}$: The diffraction angle of the (hkl) reflection.

B: The shape factor; its value ranges between 0.89 and 1 (0.9 for isotropic or nearly isotropic crystallites).

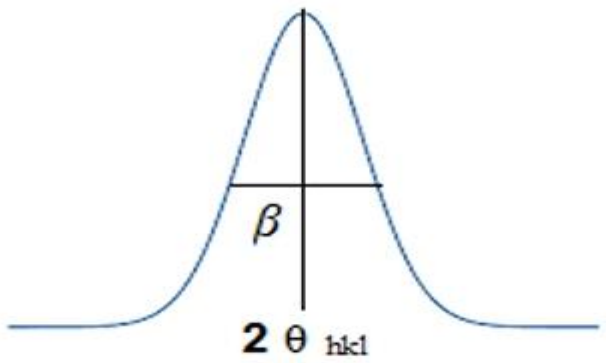

Figure II.8: Schematic representation of a diffraction peak

The optimisation of the lattice parameters and the zero-shift is achieved with the equation for a cubic unit cell:

$$a_0 = d\sqrt{(h^2+k^2+l^2)}$$

Where *d* represents the interplanar spacing determined using the Wulff-Bragg relation.[8]

II.2.2 Spectroscopie UV-visible

II.2.2.1. Principle of ultraviolet (UV) absorption spectra

is derived from the excitation of electrons within a molecule or an ion transitioning from a lower energy state to a higher energy state, whereas the UV emission spectra result from the reverse transition. Ultraviolet radiation possesses adequate energy to facilitate the promotion or excitation of valence electrons in a molecule or ion from a ground state orbital to a higher energy level, known as an excited state orbital or an anti-bonding orbital, which manifests as absorption .

Chromophores: Numerous organic molecules exhibit the capacity to absorb ultraviolet or visible radiation, primarily due to the presence of specific functional groups. The functional groups responsible for the absorption of radiation are designated as chromophores. Certain electronic transitions are statistically favored and exhibit considerable intensity, while other transitions possess a zero probability and are

categorized as forbidden; however, several particularly significant forbidden transitions include d→d absorptions of transition metals, the n→π* absorption of carbonyl groups at approximately 280 nm, and the π→π* absorption of aromatic compounds between approximately 230–330 nm, contingent upon the substituents on the benzene ring .

Auxochromes: The coloration of a molecule may be enhanced by functional groups referred to as auxochromes, which typically do not exhibit significant absorption in the 200-800 nm range but influence the spectrum of the chromophore to which they are bound. The most notable auxochromic groups include OH, NH2, CH3, and NO2, with properties that are either acidic (phenolic) or basic. The actual impact of an auxochrome on a chromophore is contingent upon the polarity of the auxochrome; for instance, groups such as CH3- demonstrate this effect. Generally, it is feasible to anticipate the influence of non-polar or weakly polar auxochromes, whereas the effects of strongly polar auxochromes remain challenging to predict.

Solvents: The influence on the absorption spectrum of a compound when diluted in a solvent varies in accordance with the involved chemical structures. Typically, non-polar solvents and non-polar molecules exhibit minimal effects. Conversely, polar molecules demonstrate significant variations when interacting with a polar solvent. The interaction between the solute and solvent results in absorption band broadening and a subsequent decrease in structural resolution and ε max. Therefore, it is imperative to exercise caution to prevent interactions between the solute and the solvent. Water and 0.1N solutions of hydrochloric acid (HCl) and sodium hydroxide (NaOH) are frequently utilized solvents in absorption spectrometry. The methodology necessitates buffering, with solutions required to be non-absorbing, and typically both the composition and pH must be specified. For reactions occurring within the pH range of 4.2 to 8.8, mixtures of 0.1N dihydrogen sodium phosphate and 0.1N hydrogen disodium phosphate are customarily employed .

Potentially, three ground state orbitals are implicated: σ (bonding) molecular orbital, π (bonding) molecular orbital, and n (non-bonding) atomic orbital. Correspondingly, the anti-bonding orbitals involved consist of the σ* orbital and π* orbital. There exists no n* anti-bonding orbital, as the n electrons do not participate in bonding [8]. Subsequently, the potential electronic transitions in the ultraviolet and visible regions are delineated as follows:

1. σ to σ*
2. n to σ*
3. n to π*
4. π to π*

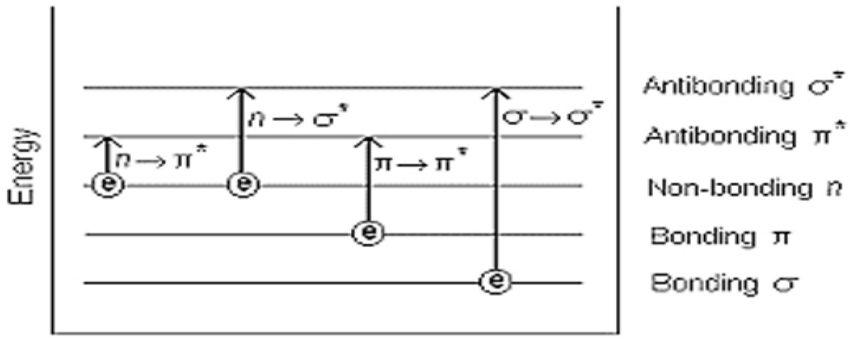

Figure 1 : Electronic transitions

II.2.2.2. Beer Lambert's Law :

Different molecules absorb varying quantities of energy, which can be illustrated through a graph featuring absorbance on the y-axis and wavelength on the x-axis. This graph is commonly known as an absorption spectrum. By identifying the λmax (the wavelength at which the sample exhibits peak absorbance) of the sample, we can subsequently ascertain the concentration. This process is fundamentally grounded in the principle of Beer-Lambert's Law, which asserts that 'the absorbance of a sample is directly proportional to the concentration of the absorbing species and the path length.

$$A = \varepsilon c l$$

Where :

A : Absorbance,

ε : molar extinction coefficient,

c : concentration of the absorbing species,

l : path length

With a constant path length, this principle can be utilized to calculate the concentration of an absorber within a sample. Therefore, it is crucial to understand how swiftly the absorbance varies with changes in concentration.[9]

II.2.3 Infrared spectroscopy

The examination of infrared absorption phenomena in inorganic solids facilitates the recognition of specific functional groups and yields structural insights based on their vibrational characteristics. Infrared radiation stimulates distinct and characteristic vibrational modes (such as bending and stretching) of chemical bonds. By analyzing the incident radiation alongside the transmitted light through the sample, one can ascertain the chemical species present within it.

The infrared spectrum is segmented into three distinct regions: near IR (15,600–4,000 cm^{-1}), mid IR (4,000–400 cm^{-1}), and far IR (400–40 cm^{-1}). Each of these segments necessitates specialized sources, detection systems, and beam splitters. The infrared range from 4,000 to 400 cm^{-1} pertains to the vibrational region of molecules. Not all molecular vibrations lead to absorption; this phenomenon is also influenced by the molecular geometry, particularly its symmetry.

The placement of absorption bands is primarily influenced by the differences in electronegativity between atoms and their respective masses. Consequently, for a substance with a defined chemical composition and structure, there exists a unique set of absorption bands that can be utilized to identify that substance.

The apparatus employed in this study is a Fourier Transform Infrared (FTIR) spectrometer, specifically the Shimadzu FTIR-8400 PC model, located in the chemistry laboratory at the University of Biskra. The sample preparation method utilized is

the pellet technique, which involves blending 1 mg of the sample to be examined with an excess of potassium bromide (KBr). This mixture (300 mg KBr / 1 mg powder) is subsequently compressed under pressure to create a pellet.[10]

REFERANCE

[1] A. Soufi, H. Hajjaoui, R. Elmoubarki, M. Abdennouri, S. Qourzal, N. Barka, Spinel ferrites nanoparticles: Synthesis methods and application in heterogeneous Fenton oxidation of organic pollutants – A review, Applied Surface Science Advances, **6**, 100145 (2021).

[2] É. Berrier, Structural study of phosphorescent materials doped with rare earths – Application to the development of materials based on strontium aluminate doped with europium and dysprosium, PhD thesis, University of Science and Technology of Lille, France (2005)

[3] I. Chibane, Synthesis and characterization of a pure and doped $CdCr_2O_4$ nanocomposite prepared by sol-gel method, Mémoire de Master, Université Ibn Khaldoun – Tiaret, Algérie (2019).

[4] O. Fesenko, L. Yatsenko (Eds.), Nanophysics, Nanomaterials, Interface Studies, and Applications: Selected Proceedings of the 4th International Conference Nanotechnology and Nanomaterials (NANO2016), August 24–27, 2016, Lviv, Ukraine, Springer International Publishing, Vol. **195** (2017).

[5] R. Guinebretière, Diffraction des rayons X sur échantillons polycristallins, 2ème édition, (2006).

[6] P. Scherrer, Bestimmung der Größe und der inneren Struktur von Kolloidteilchen mittels Röntgenstrahlen, Nachrichten von der Gesellschaft der Wissenschaften zu Göttingen, Mathematisch-Physikalische Klasse, **1918**, 98–100 (1918).

[7] R. Didier, P. Grecias, Exercices et problèmes de chimie générale spé, 2ème édition, Éditions Dunod (1997).

[8] A. Mandru, J. Mane, R. Mandapati, A Review on UV-visible spectroscopy, (2023).

[9] D. Sahnoune, Synthèse et propriétés physicochimiques d'oxydes de structure spinelle, Thèse de doctorat, Université Mohamed Khider – Biskra, Algérie (2022)

Chapter III: Results and Discussions

II.1. Introduction

In this chapter, we outline the steps of each method used for powder synthesis and provide a detailed discussion of the results obtained.

III.2. Preparation of $Ca_{1-x}Mg_xFe_2O_4$ Oxide by the Sol-Gel Method

he compound $Ca_{1-x}Mg_xFe_2O_4$ was synthesized for x = 0 and x = 0.25 using the sol-gel method, as illustrated in the figure III.1. In this process, citric acid ($C_6H_8O_7 \cdot H_2O$) was used as a complexing agent, following the stoichiometric balance condition:

$$n(\text{metal cations})=n(\text{citric acid})$$

In this experiment, stoichiometric amounts of $Ca(NO_3)_2 \cdot 4H_2O$, $Mg(NO_3)_2 \cdot 6H_2O$, and $Fe(NO_3)_3 \cdot 9H_2O$ were dissolved in distilled water. The solutions were mixed in a beaker and stirred while being heated to a temperature of 85–90°C.

Citric acid was gradually added to the mixture while maintaining the same temperature range until a gel was formed. The gel was then placed in a drying oven at 100°C for 24 hours to eliminate residual moisture.

After drying, the sample was finely ground and subjected to calcination at 900°C for 6 hours using an electric furnace, with a heating rate of 3°C/min

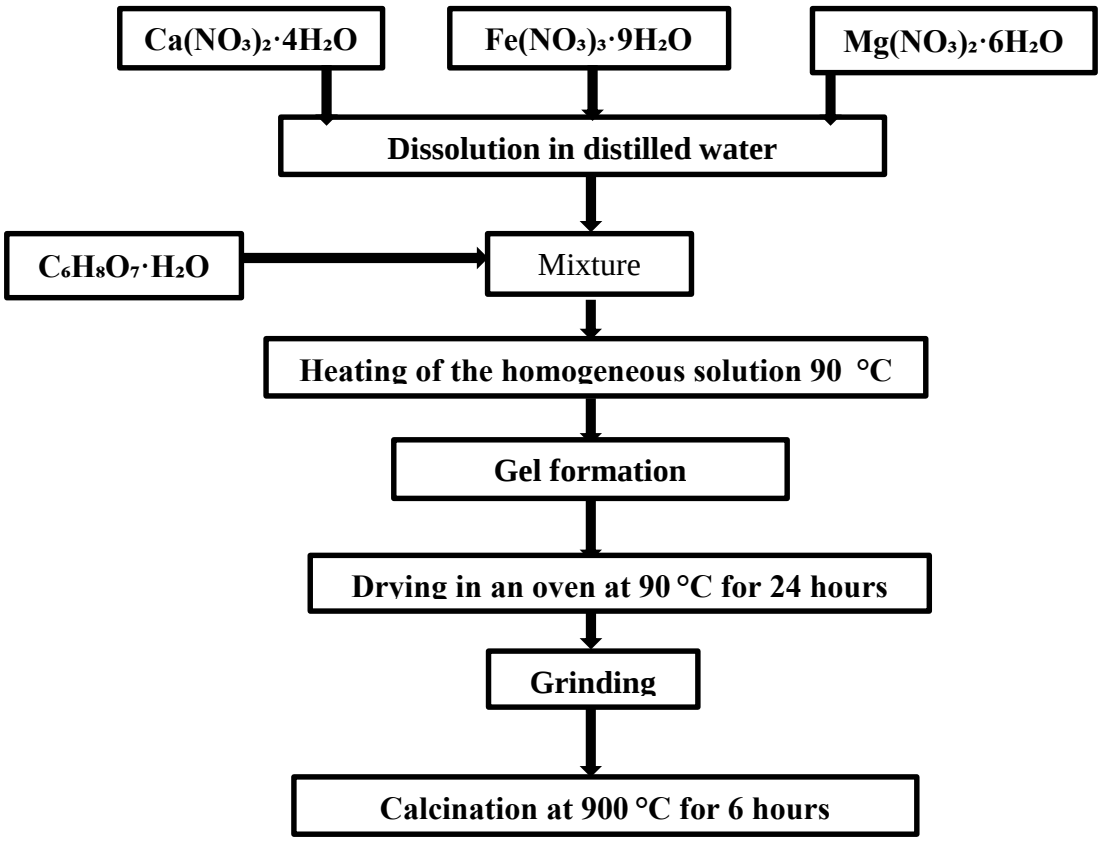

Fig. III.1: The different steps of sample synthesis via the sol-gel method

III.3. Structural Characterization of $Ca_{1-x}Mg_xFe_2O_4$ Powders

III.3.1. X-ray Diffraction Analysis

X-ray diffraction (XRD) analysis was performed using a Bruker D8 Advance diffractometer on the synthesized compound Ca1-xMgxFe2O4 for x = 0 and x = 0.25 in powder form. The measurements were carried out using Cu-Kα radiation (λ ≈ 1.5406 Å) over a 2θ range from 10° to 90°.

the obtained XRD patterns, shown in Figure (III-2), were used to analyze the crystal structure and chemical composition of the material. The powder was synthesized via the sol-gel method, dried, and then calcined at 900°C for 6 hours.

These patterns allowed us to identify the crystal structure of the prepared $CaFe_2O_4$ compound. Phase identification was carried out using the HighScore Plus software, and the main diffraction peaks were found to correspond to the spinel ferrite phase of calcium, as confirmed by matching with standard PDF cards [01-072-1199]. The compound crystallizes in an orthorhombic crystal system with a Pnma space group.

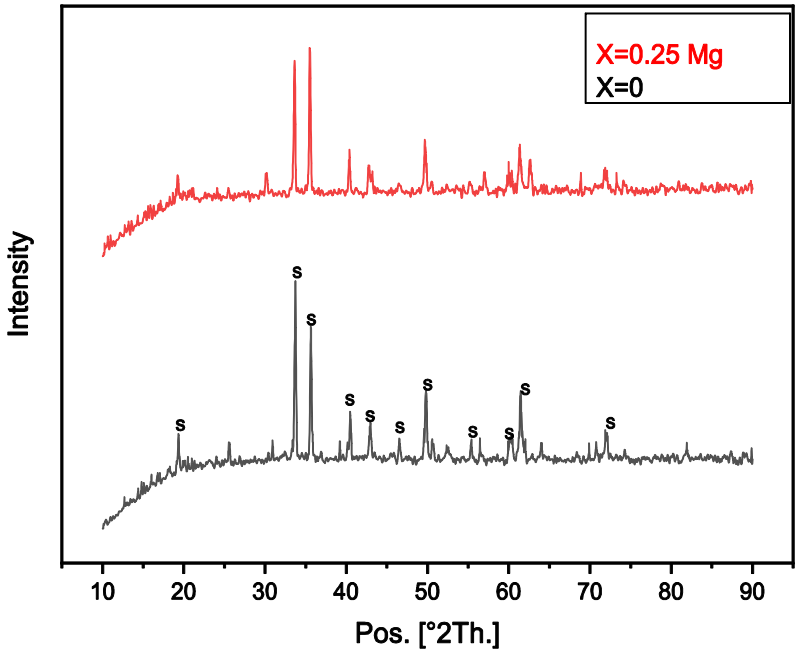

Fig. III.2 : XRD patterns of $Ca_{1-x}Mg_xFe_2O_4$ oxides x = 0 and x = 0.25 ;S spinel

Figure III-3 shows the most intensive diffraction peak of Mg- doped CaFe2O4, with 2θ around 33.7601° . This peak shifts to lower angles with increasing Mg content. This is due to the incorporation of Mg+2 into the spinel structure.

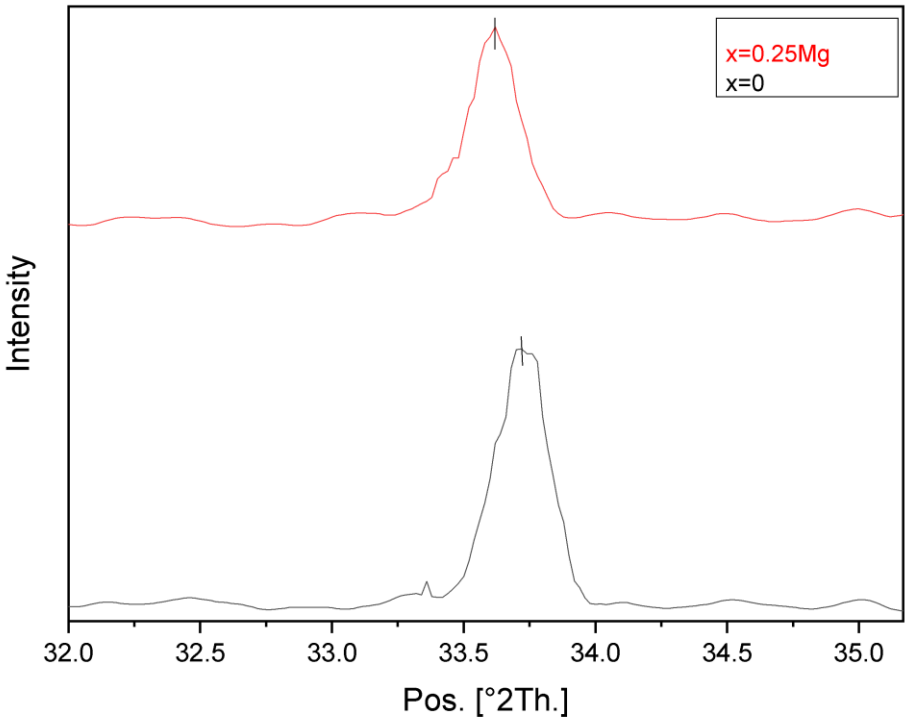

Fig. III.3. Evolution of the the most intensive diffraction peak position

The phase compositions, lattice parameters and unit cell volumes of the investigated samples $0 \leq x \leq 0.25$ after heat treatment at (900°C) are summarized in tableIII- 1. The lattice parameters and volume of the spinel decrease slightly with increasing of x from 0 to 0.25.

Samples	**lattice parameters A≠B≠C (Å)**			**Unit cell volumes (Å^3)**
	A	**B**	**C**	
$CaFe_2O_4$	8.917	10.6201	3.14	297.9004
$Ca_{0.75}Mg_{0.25}Fe_2O_4$	8.9369	10.669	3.0896	294.5769

Table III- 1: Crystallographic parameters of oxides

This variation due to the substitution of Ca+2 with ionic radius r =1.00A by Mg+2 with ionic radius r = 0.72 A . Similar tendency has been found previously for Mg1-xCax Fe2O4 samples. [1]

The values of the average crystallite sizes for the oxides CaFe2O4 and Ca0.75Mg0.25Fe2O4 are grouped in Table III.2, below

Sample	Position of the most intense peak 2θ(°)	Average crystallite size D (nm
$CaFe_2O_4$	33.7601	60.26086
$Ca_{0.75}Mg_{0.25}Fe_2O_4$	33.6007	52.7294

Table III.2: Average crystallite size for Ca0.75Mg0.25Fe2O4 oxides

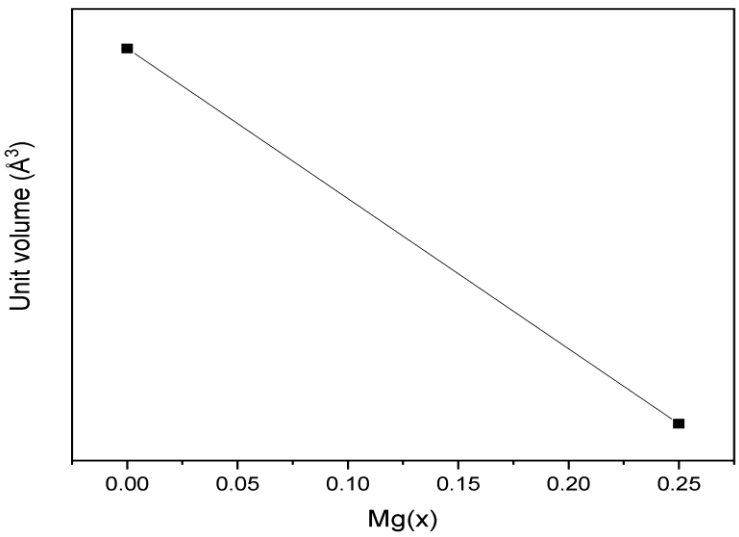

Fig. III.4: Evolution of crystallite size as a function of calcium content (x)

III 3.2. Analyse par spectroscopie infrarouge

The FTIR spectra were recorded for both the pure $CaFe_2O_4$ compound (X = 0) and the doped with 25% magnesium ions (X = 0.25 Mg) to study the effect of doping on the structural composition of the compound. A similarity between the two spectra was observed, as shown in **Figure III.5**.

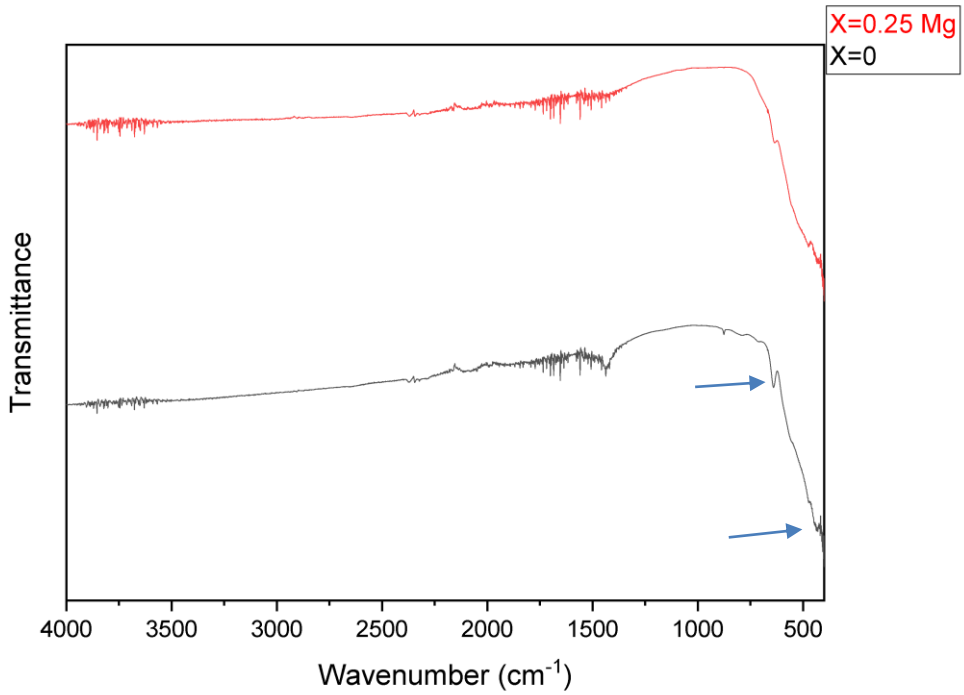

Figure III.5 : Infrared Spectra of $Ca_{1-x}Mg_xFe_2O_4$ Oxides ($0 \leq x \leq 0.5$)

From the spectra, two main bands were observed in the FTIR spectrum:

Two characteristic bands of the spinel phase appear, one around 500 cm^{-1} and the other at about 690–700 cm^{-1} **[2,3].** The band around 700 cm^{-1} is attributed to the stretching vibration mode of the M–O bond in the tetrahedral sites, while the band around 500 cm^{-1} corresponds to the vibrations of the M–O lattice in the octahedral sites **[4].** These results confirm the formation of a stable spinel structure in the analyzed samples.

III.3.3. Analyses par uv

The optical properties of the compound $Ca_{1-x}Mg_xFe_2O_4$ (where x = 0 and 0.25) were analyzed using a UV-Vis spectrophotometer in the wavelength range of 200 to 800 nm to determine the optical band gap. Two absorption curves were obtained, as shown in Figure III.6-7

The absorption spectra show two characteristic bands in the UV region around 255 and 320 nm as well as a notable absorption in the visible region at around 550 nm, indicating that our material has visible light absorption capacity, which is essential for photocatalysis applications [5,6].

These measurements allow for the determination of the optical band gap (Eg) of the synthesized materials, which is related to the energy of the incident photon (hν), as described by Tauc's law:

$$(\alpha h\nu)1/n = A\ (h\nu - Eg\ )$$

where α is the absorption coefficient, A is a constant, Eg is the optical bandgap of the material, and the exponent (n) depends on the nature of the electronic transition.

The band gap was calculated by analyzing the linear region of the $(\alpha h\nu)^2$ versus photon energy (hν) plot. This analysis involves extrapolating the linear part of the curve to intersect with the energy axis.

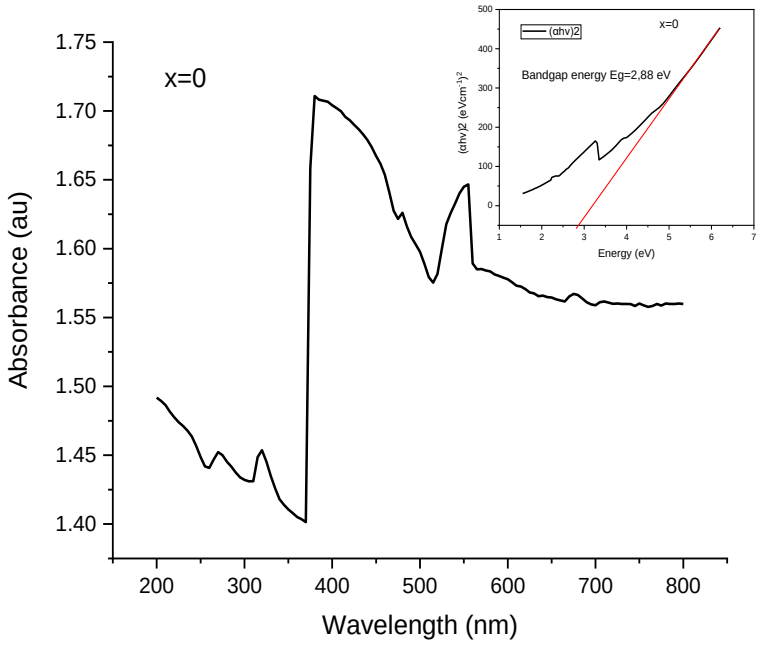

Figure III.6: optical absorption spectra of $CaFe_2O_4$ oxides calcined at (900°C)

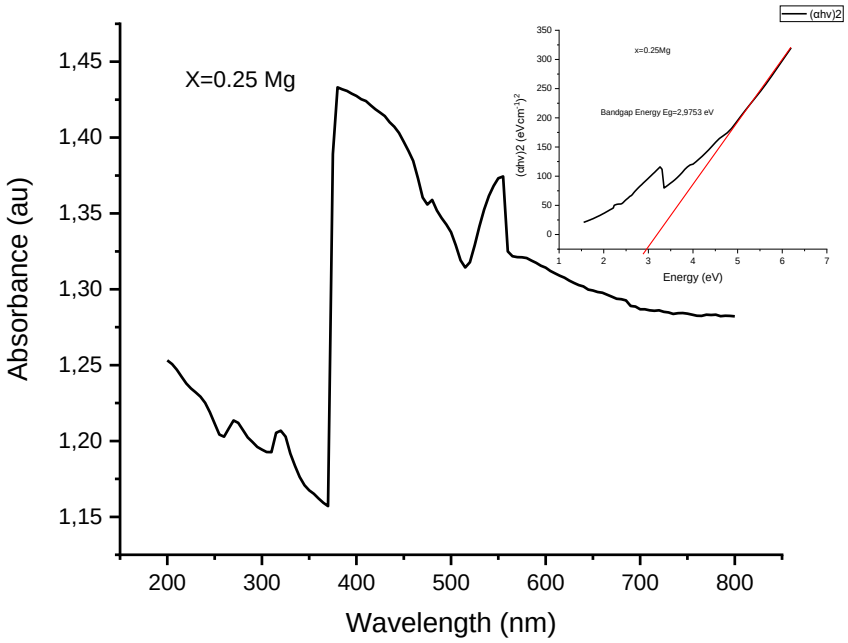

Figure III.7.: optical absorption spectra of $Ca_{0.75}Mg_{0.25}Fe_2O_4$ oxides calcined at (900°C)

The results show a value of 2.88 eV for $CaFe_2O_4$ and a notable increase to 2.97 eV for $Ca_{0.75}Mg_{0.25}Fe_2O_4$, which confirms the effect of partial substitution of Ca2+ by Mg2+ in the crystal structure, thus modifying the band gap and electronic properties of the material [7,8].

This increase in the optical gap with Mg doping due to the contraction of the particle size, which could be due to a quantum confinement effect [9]. The Eg value of the pure CaFe2O4 sample is 2.88 eV, which corresponds to the blue shift of the Mg-doped samples (Eg =2.97 eV) which indicates that the Ca1-xMgxFe2O4 samples could exhibit photocatalytic activity in visible light.

References

[1] Influence of Ca2+ Ion Substitution on Structural, Morphological, Optical, Thermal and Magnetic Behaviour of Mg1-xCaxFe2O4 (0 ≤x≤0.5) Spinel, Journal of Superconductivity and Novel Magnetism. https://doi.org/10.1007/s10948-020-05665-1

[2]. Ristic, M., Music, S., Popovic, S., et al., "Thermal behavior and structural characteristics of $NiFe_2O_4$ powders," Journal of Molecular Structure, vol. 744–747, pp. 535–540,(2005).

[3]. El-Sayed, M.M., "FTIR and structural investigations of nanocrystalline $MgFe_2O_4$ spinel ferrite," Journal of Alloys and Compounds, vol. 486, pp. 759–764, (2009).

[4]. Choudhary, R.J., Lalla, N.P., et al., "Infrared study on nanocrystalline Fe_3O_4 and γ-Fe_2O_3 obtained by mechanochemical synthesis," Journal of Applied Physics, vol. 95, pp. 7452–7455, (2004).

[5]. Berdous, D., Kenfoud, H., & Trari, M. Physico-chemical properties of the spinel $CaFe_2O_4$ synthesized by sol–gel route: application to drimarene green X-3G photodegradation. Reaction Kinetics, Mechanisms and Catalysis, 136, 507–522 (2022).

[6]. Shankar, P., Raveendra, R. S., Jayasheelan, A., Prakash, C. S., Nagabhushana, B. M., Nagabhushana, H., & Prasad, B. D. Synthesis, characterization and magnetic properties of $CaFe_2O_4$ nanoparticles by solution combustion method. International Journal of Advanced Scientific and Technical Research, 5(1), 1–10.(2015)

[7]. Alhassan, S., et al. Preparation and Optical Properties of PVDF-$CaFe_2O_4$ Polymer Nanocomposite Films. Polymers, 15(9), 2232.(2023)

[8]. Trari, M., & Rhouma, A. Effect of Pb doping on the structural and optical properties of ferrite materials. Journal of Materials Science: Materials in Electronics, 28(6), 4518–4526 (2017).

[9]. G. Mathubala, S. Prabhu, R. Rajeswari, Photocatalytic degradation of methylene blue dye and magneto optical studies of magnetically recyclable spinel NixMn1−xFe2O4 (x = 0.0–1.0) nanoparticles, J. Mol. Struct. **1113**, 79–87 (2016).

General Conclusion

in this study, our contribution focused on the preparation and investigation of the properties of a spinel compound $Ca_{1-x}Mg_xFe_2O_4$ (where x = 0 and 0.25) We synthesized our compound using the sol-gel method followed by calcination at 900 °C. The material was then characterized using several analytical techniques, including X-ray diffraction (XRD), Fourier-transform infrared spectroscopy (FTIR), and UV-visible spectroscopy (UV-Vis).

The XRD analysis revealed that the incorporation of magnesium ions (Mg^{2+}) led to a decrease in both the unit cell volume and the lattice parameters. It also caused a reduction in the crystallite size, indicating a noticeable impact on the crystal structure due to Mg^{2+} substitution.

FTIR spectra showed the presence of two characteristic bands: one around 500 cm^{-1} and another between 690–700 cm^{-1}.The band near 700 cm^{-1} is attributed to the stretching vibrations of the metal–oxygen (M–O) bond in tetrahedral sites, whereas the band near 500 cm^{-1} corresponds to M–O vibrations in octahedral sites.

UV-Vis absorption spectra exhibited two prominent bands in the ultraviolet region, centered around 255 nm and 320 nm, along with a significant absorption band in the visible region at approximately 550 nm. This visible light absorption indicates that our material possesses potential photocatalytic activity.

Moreover, the optical band gap was found to increase, confirming the effect of the partial substitution of Ca^{2+} by Mg^{2+} on the crystal structure and electronic properties of the material

Abstract

The compound $Ca_{1-x}Mg_xFe_2O_4$ (with x = 0 and x = 0.25), which belongs to the spinel ferrite family, was synthesized using the sol-gel method in order to investigate the effect of magnesium substitution on its properties. The prepared samples were characterized using various techniques, including X-ray diffraction (XRD), Fourier-transform infrared spectroscopy (FTIR), and UV-Visible spectroscopy (UV-Vis). The results showed an increase in the optical band gap in the studied samples, indicating that the $Ca_{1-x}Mg_xFe_2O_4$ compound may exhibit photocatalytic activity under visible light.

Keywords : Sol-gel method , X-ray diffraction (XRD) , Infrared spectroscopy (FTIR) UV-Visible spectroscopy (UV-Vis) , Optical band gap

Résumé

Le composé $Ca_{1-x}Mg_xFe_2O_4$ (avec x = 0 et x = 0,25), appartenant à la famille des ferrites de type spinelle, a été synthétisé par la méthode du sol-gel afin d'étudier l'effet de la substitution du calcium par le magnésium sur ses propriétés. Les échantillons préparés ont été caractérisés à l'aide de différentes techniques, notamment la diffraction des rayons X (DRX), la spectroscopie infrarouge à transformée de Fourier (FTIR) et la spectroscopie UV-Visible (UV-Vis). Les résultats ont montré une augmentation de la bande interdite optique, ce qui indique que le composé $Ca_{1-x}Mg_xFe_2O_4$ pourrait présenter une activité photocatalytique sous la lumière visible.

Mots–clés : Méthode sol-gel , Diffraction des rayons X (DRX) , Spectroscopie infrarouge (FTIR) , Spectroscopie UV-Visible (UV-Vis) , Bande interdite optique

ملخص

تم تحضير مركب) $Ca_{1-x}Mg_xFe_2O_4$ بـ $x = 0$ و $x = 0.25$) من نوع سبينل فيريت باستخدام طريقة السول-جيل، بهدف دراسة تأثير إدخال المغنزيوم على خصائصه البنيوية والبصرية. تم تشخيص العينات المحضّرة باستخدام تقنيات متعددة، مثل حيود الأشعة السينية(XRD) ، والتحليل بالأشعة تحت الحمراء(FTIR) ، والأشعة فوق البنفسجية-المرئية (UV-Vis).أظهرت نتائج التحليل أن إدخال المغنزيوم يؤدي إلى زيادة في فجوة الطاقة البصرية، مما يشير إلى أن مركب $Ca_{1-x}Mg_xFe_2O_4$ قد يُظهر نشاطًا فوتوكاتاليتيًا تحت الإضاءة المرئية

الكلمات مفتاحية • **:**طريقة السول جل , حيود الأشعة السينية, التحليل بالأشعة تحت الحمراء التحليل بالأشعة فوق البنفسجية , فجوة الطاقة البصرية

République Algérienne Démocratique et Populaire
Ministère de l'Enseignement Supérieur et de la Recherche Scientifique
Université Med Khider Biskra

Faculté des Sciences Exactes
Département des Sciences de la Matière
Filière de Chimie

الجمهورية الجزائرية الديموقراطية الشعبية
وزارة التعليم العالي و البحث العلمي
جامعة محمد خيضر بسكرة

كلية العلوم الدقيقة
قسم علوم المادة
شعبة الكيمياء

تصريـح شرفـــي

خاص بالالتزام بقواعد النزاهة العلمية لإنجاز بحث

(ملحق القرار 1082 المؤرخ في 2021/12/27)

أنا الممضي أسفله،

السيد(ة) مداس زكرياء

الصفة: طالب سنة ثانية ماستر كيمياء تخصص: كيمياء مواد

الحامل(ة) لبطاقة التعريف الوطنية رقم: 205903962 الصادرة بتاريخ: 2020

المسجل بكلية: كلية العلوم الدقيقة و علوم الطبيعية والحياة قسم: علوم المادة والمكلف

بانجاز أعمال بحث : مذكرة ماستر في الكيمياء

عنوانها: Physical and chemical properties of spinal oxide doped with magnesuim

.....

أصرح بشرفي أني ألتزم بمراعات المعايير العلمية والمنهجية ومعايير الأخلاقيات المهنية والنزاهة الاكاديمية المطلوبة في انجاز البحث المذكور أعلاه وفق ما ينص عليه القرار رقم 1082 المؤرخ في 2021/12/27 المحدد للقواعد المتعلقة بالوقاية من السرقة العلمية ومكافحتها.

التاريخ: 2025/05/25

إمضاء المعني بالمر

ZAKI